

# Physical modelling and similitude of air bubble entrainment at vertical circular plunging jets

H. Chanson<sup>a,\*</sup>, S. Aoki<sup>b</sup>, A. Hoque<sup>b</sup>

<sup>a</sup>Department of Civil Engineering, The University of Queensland, Brisbane, QLD 4072, Australia

<sup>b</sup>Toyohashi University of Technology, Tempaku-cho, Toyohashi 441-8580, Japan

Received 16 July 2002; received in revised form 14 November 2003; accepted 20 November 2003

## Abstract

When a plunging jet impinges into a pool of liquid, air bubble entrainment takes place if the inflow velocity exceeds a threshold velocity. This study investigates air entrainment and bubble dispersion in the developing flow region of vertical circular plunging jets. Three scale models were used and detailed air–water measurements (void fraction, bubble count rate, bubble sizes) were performed systematically for identical inflow Froude numbers. The results highlight that the modelling of plunging jet based upon a Froude similitude is affected by significant scale effects when the approach flow conditions satisfied  $We_1 < 1E + 3$ , while some lesser scale effect was noticed for  $V_1/u_r < 10$  and  $We_1 > 1E + 3$ . Bubble chord time measurements showed pseudo-chord sizes of entrained bubbles ranging from less than 0.5 mm to more than 10 mm with an average pseudo-chord size were between 4 and 9 mm. However, bubble size data could not be scaled properly. © 2003 Elsevier Ltd. All rights reserved.

**Keywords:** Air bubble entrainment; Circular plunging; Similitude; Physical modelling; Developing shear flow

## 1. Introduction

### 1.1. Presentation

At the intersection of a plunging jet with a pool of water, free-surface instabilities develop and air bubble entrainment may be observed (Fig. 1). This is a form of local, singular aeration (see review by Bin, 1993; Chanson, 1997). Plunging jet flow situations are encountered in Nature (e.g. at impact of waterfalls). Industrial applications of plunging jets include minerals-processing floatation cells, waste-water treatment, oxygenation of mammalian-cell bio-reactors and riverine re-oxygenation weirs (e.g. Goldring et al., 1980; Robison, 1994; Chanson, 1997). In each case a strong mixing process takes place. A related case is the air entrainment by a plunging solid surface in a liquid bath. Such a configuration is used for polymer coating, in the production of photographic film, and it is observed at the impact of a missile with a free-surface (e.g. Knapp et al., 1970; Kennedy and Burley, 1977).

### 1.2. Bibliographic review

Several studies showed that air entrainment at plunging jets takes place when the jet impact velocity exceeds a characteristic velocity  $V_e$  which is a function of the inflow conditions (e.g. McKeogh, 1978; Cummings and Chanson, 1999). The mechanisms of bubble entrainment depends upon the jet velocity at impact, the physical properties of fluid, the jet nozzle design, the length of free-falling jet and the jet turbulence (Bin, 1993). For small jet velocities larger than a threshold velocity, called onset velocity, air is entrained in the form of individual air bubbles. At larger jet velocities, large packets of air are entrained and broken up subsequently in the shear flow (e.g. Bin, 1993; Cummings and Chanson, 1997a; Chanson and Brattberg, 1998; Zhu et al., 2000). Flow patterns at two-dimensional plunging jet flows were investigated by Goldring et al. (1980) and Sene (1988). Cummings and Chanson (1997a, b); Chanson and Brattberg (1998) and Brattberg and Chanson (1998) presented detailed measurements of air content and velocity distributions in developing flows.

Several researchers showed interest in circular plunging jets (e.g. reviews by Bin, 1993; Chanson, 1997). Numerous experiments were performed with small circular jets

\* Corresponding author. Tel.: +61-733-65-41-63; fax: +61-733-65-45-99.

E-mail address: h.chanson@mailbox.uq.edu.au (H. Chanson).



Fig. 1. Photograph of air bubble entrainment at a vertical circular plunging jet ( $V_1 = 3.3$  m/s,  $x_1 = 0.5$  m, Model 2).

(i.e. less than 5 mm diameter) for which mostly qualitative studies were performed. Only a small number of researchers studied the flow field below impingement. McKeogh and Ervine (1981) and Van de Donk (1981) recorded air concentration profiles and velocity distributions primarily in the fully developed flow region while Bonetto and Lahey (1993) presented results obtained in both developing and fully developed flow regions. Bin (1993) and Chanson (1997) highlighted the lack of information on the air content distributions in the vicinity of the impingement point and on the entrained bubble size distributions. Further, physical modelling of plunging jet flows remains subject to scaling effects which have not properly explained (e.g. Wood, 1991; Chanson, 1997).

This study investigates basic air entrainment characteristics at vertical circular plunging jets. Three scale models were built and detailed experiments were performed for a wide range of flow situations. The results presents new evidence leading to a better understanding of scale effects

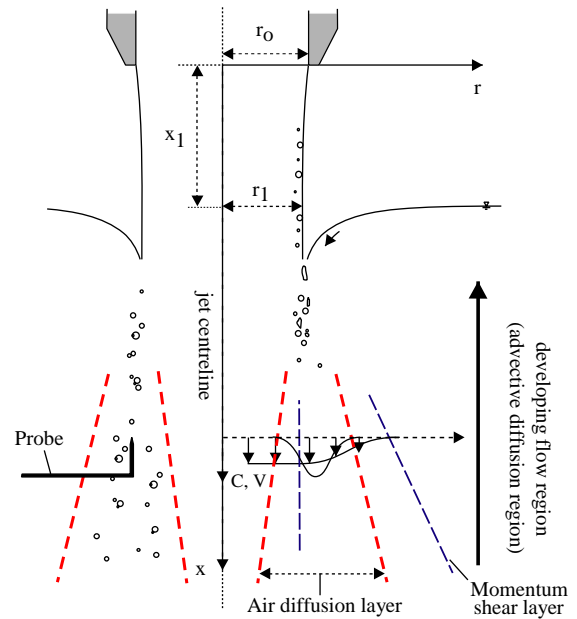


Fig. 2. Sketch of air entrainment at vertical circular plunging jet.

affecting the air entrainment process at circular vertical plunging jets.

## 2. Dimensional analysis

Laboratory studies of air–water flows require the selection of an adequate similitude. Considering air bubble entrainment at plunging water jets, the relevant parameters needed for any dimensional analysis include fluid properties and physical constants, channel (or flow) geometry, upstream flow properties, air–water flow properties. A simplified analysis for vertical circular plunging jets yields

$$C, Fr, Tu, \frac{d_{ab}}{d_1} \dots = F \left( \frac{x - x_1}{d_1}; \frac{r}{d_1}; \frac{x_1}{d_1}; Fr_1; We_1; Tu_1; Mo \dots \right), \quad (1)$$

where  $C$  is the void fraction,  $Fr = V/\sqrt{gd_1}$ ,  $V$  is the velocity,  $d_1$  is the jet impact diameter,  $Tu$  is a turbulence intensity, and  $d_{ab}$  is a characteristic size of entrained bubble at a distance  $(x - x_1)$  beneath the free-surface and a radial distance  $r$ , where  $x$  is the distance from the nozzle and  $x_1$  is the free-jet length (Fig. 2). The dimensionless inflow variables are  $x_1/d_1$ ,  $Fr_1 = V_1/\sqrt{gd_1}$ ,  $We_1 = \rho_w V_1^2 d_1/\sigma$  and  $Tu_1$  while  $Mo = (g\mu_w^4)/(\rho_w\sigma^3)$  is the Morton number also called liquid parameter. Eq. (1) expresses that the dimensionless characteristics of the air–water flow field below impingement (e.g.  $C, Fr, Tu, d_{ab}/d_1$ ) are functions of the inflow conditions.

In free-surface flows, gravity effects are important and most laboratory studies are based upon a Froude similitude (e.g. Henderson, 1966; Hughes, 1993; Chanson, 1999).

Table 1  
Experimental investigations of vertical, circular plunging jet flows

Ref. (1)	$d_o$ (m) (2)	$x_1$ (°) (m) (3)	$V_1$ (m/s) (4)	$Fr_1$ (m) (5)	$Tu_1$ (6)	Inception conditions (7)	Comments (8)
M1	0.025	0.1				$V_e = 1.58$ m/s	Tap water, $\mu_w = 1.015E - 3$ Pa s, $\sigma = 0.055$ N/m. Inflow pipe: 3.5 m long, 0.054 m diameter. Water depth: $\sim 1.5$ m.
			3.5	7.2	0.39%	$(Tu_1 = 0.47\%)$	
			4.1	8.4	0.46%		
			4.4	9.0	0.96%		
M2	0.0125	0.05			N/A	$V_e = 1.03$ m/s	Tap water, $\mu_w = 1.22E - 3$ Pa s, $\sigma = 0.073$ N/m. Inflow pipe: 1.2 m long, 0.0125 m diameter. Water depth: $\sim 0.65$ m.
			2.42	7.1			
			3.04	8.8			
			3.18	9.2			
			3.46	10.0			
M3	0.00683	0.0273			N/A	$V_e = 0.73$ m/s	Tap water, $\mu_w = 1.22E - 3$ Pa s, $\sigma = 0.073$ N/m. Inflow pipe: 1 m long, 0.00683 m diameter. Water depth: $\sim 0.65$ m.
			1.79	7.1			
			2.16	8.5			
			2.30	9.0			
			2.49	9.7			

Notes:  $Tu_1$ : turbulence intensity of the jet core at impact;  $\mu_w$ : measured dynamic viscosity of water;  $\sigma$ : measured surface tension between air and water;  $x_1$ : longitudinal distance between the nozzle and the free-surface pool; N/A: information not available.

That is, the Froude number must be identical in model and prototype. The entrainment of air bubbles and the mechanisms of air bubble breakup and coalescence are dominated by surface tension effects implying the need for Weber similitude. For geometrically similar models, it is impossible to satisfy simultaneously Froude and Weber similarities. In small size models, the air entrainment process may be affected by significant scale effects. Wood (1991) and Chanson (1997) presented comprehensive reviews. Kobus (1984) illustrated some applications.

Eq. (1) demonstrates that dynamic similarity of air entrainment at plunging jets is impossible with geometrically similar models. In the present study, geometrically similar models of circular vertical plunging jets were designed based upon a Froude similitude with undistorted scale. The geometric scaling ratio between Models 1 and 2 was 2.0, and the scaling ratio was 3.66 between Models 1 and 3. Similar experiments were conducted for identical inflow Froude numbers  $Fr_1$ . Measurements were performed at similar cross sections  $(x - x_1)/r_1$  where  $x$  is the longitudinal coordinate and  $r_1$  is the jet impact radius ( $r_1 = d_1/2$ ) (Fig. 2).

### 3. Experimental apparatus and instrumentation

#### 3.1. Presentation

Three circular plunging jet configurations, called Models 1–3, were used (Table 1, Fig. 1). Experiments were con-

ducted with tap water and ambient air. In Model 1, the jet nozzle was made of aluminium with a 1/2.16 contraction ratio, the nozzle diameter was 25 mm and the receiving channel was 0.3 m wide and 1.8 m deep. In Models 2 and 3, the nozzle was a sharp-edged, machined PVC pipe (i.e. 1:1 contraction ratio), the nozzle diameter was 12 and 6.83 mm, respectively, and the receiving flume was 0.10 m wide and 0.75 m deep (Fig. 1). The dimensionless free-jet length was identical for all experiments (Table 1, Column 3).

#### 3.2. Instrumentation

The discharge was measured in Model 1 with an orifice meter (British Standards design) calibrated on-site with a volume-per-time technique. The flow rate was measured with a volume per time method in Models 2 and 3. The error on the discharge measurement was less than 2%.

In Model 1, clear water jet velocities and turbulent velocity fluctuations were measured in the free-falling jet using a Prandtl-Pitot tube (diameter 3.3 mm) and a conical hot-film probe system (Dantec 55R42, 0.3 mm  $\varnothing$ ). The latter was initially calibrated with the Pitot tube data and the velocity distribution was checked with the measured flow rate within 2% for velocities ranging from 1 to 5 m/s.

Air–water flow properties were measured with single-tip conductivity probes (needle probe design). In Model 1, the probe consisted of a sharpened rod (platinum wire  $\varnothing = 0.35$  mm) which was insulated except for its tip and set

into a metal supporting tube (stainless steel surgical needle  $\varnothing = 1.42$  mm) acting as the second electrode. The probe was excited by an electronics (Ref. AS25240) designed with a response time less than 10  $\mu$ s and calibrated with a square wave generator. The probe output signal was scanned at 5 kHz for 3 min. A Kanomax<sup>TM</sup> System 7931 resistivity probe (inner electrode  $\varnothing = 0.1$  mm) was used in Models 2 and 3. The electronics had a response time estimated to be less than 30  $\mu$ s. The void fraction and bubble count rate were calculated by the Kanomax<sup>TM</sup> analog integrator during 5 min. Raw probe outputs were recorded at 25 kHz for 2.6 s to calculate bubble chord time distributions.

Conductivity probe measurements were taken on the jet diameter through the centreline. In each model and at each cross section, the probe sensor and support were initially located at  $r < -2r_1$  and measurements were conducted by moving the probe tip with increasing radial coordinate  $r$  up to over  $r > +2r_1$  where  $r_1$  is the jet impact radius. The displacement of the probes in the flow direction and direction normal to the jet support was controlled by fine adjustment travelling mechanisms. The error in the probe position was less than 0.2 mm in each direction. Additional measurements were performed using high speed photographs and movies. Further details on the experiments were reported in Chanson et al. (2002).

Water density was measured with a Nagashima<sup>TM</sup> Standard Hydrometer GI-0361-11. Dynamic viscosity was measured with a cone and plate viscosimeter Toki<sup>TM</sup> RE80 operated at controlled temperature. Surface tension was recorded using a surface wave method (e.g. Iino et al., 1985). The measured fluid properties are listed in Table 1.

### 3.3. Data processing

The void fraction  $C$  is the proportion of time that the probe tip is in the air. Past experience showed that the probe orientation with the flow direction had little effect on the void fraction accuracy provided that the probe support does not affect the flow past the tip (e.g. Sene, 1984; Chanson, 1988). This was true in Model 1 but the Kanomax<sup>TM</sup> resistivity probe was possibly affected by the probe orientation (Yasuda, 2001, Personal communication). In the present study, the probe tip was aligned with the flow direction as sketched in Fig. 2. The bubble count rate  $F$  is the number of bubbles impacting the probe tip.

The bubble chord time  $t_{ch}$  is defined as the time spent by the bubble on the probe tip. Bubble chord times were calculated at eight different locations per cross section, selected next to the location of maximum void fraction and maximum bubble frequency. The signal was processed using a single threshold technique and the threshold was set at about 15–20% of the air–water voltage range. (An incomplete sensitivity analysis was conducted with thresholds between 10% and 30% of the voltage range. The results showed little effect of the threshold on chord time results.) The results

are presented in terms of pseudo-bubble chord length  $ch_{ab}$  defined as

$$ch_{ab} = V_1 t_{ch}, \quad (2)$$

where  $V_1$  is the jet impingement velocity. Chanson et al. (2002) compared Eq. (2) with chord length measurements by Chanson and Brattberg (1996) and Cummings and Chanson (1997b). The results showed that Eq. (2) predicts the exact shape of bubble size probability distribution functions although it overestimates the bubble chord lengths by about 10–30%.

## 4. Distributions of void fractions and bubble count rates

### 4.1. Basic flow patterns

Each model exhibited similar flow patterns. In all experiments, the free jet was transparent. No entrained bubbles could be seen in the free jet although small longitudinal streaks were visible at the free-surface. For very low impact velocity, no air was entrained at jet impact. With increasing jet velocities, all the other parameters being unchanged, individual bubble entrainment was seen. The inception conditions for air bubble entrainment were measured and reported in Table 1, Column 7. The results for Models 1 and 2 were consistent with previous results (e.g. Irvine et al., 1980; Cummings and Chanson, 1999). In Model 3, the flow conditions at inception were visually different. The free jet surface was smooth, followed by free-surface annular waves developing in the flow direction similar to wavy flow patterns illustrated by Brennen (1970) and Hoyt and Taylor (1977). It is believed that the inflow was laminar.

For a jet velocity slightly greater than the inception velocity, individual air bubble entrainment was observed. Most entrapped bubbles were visually small (i.e. with diameter less than 0.5–1 mm) and tended to follow a slightly helical trajectory around the jet centreline. For larger jet velocities ( $V_1 > V_e$ ), an unstable air cavity developed at one point along the impingement perimeter. The air cavity position changed with time in an apparently random manner. Large air packets were entrained below the air cavity with the stretching and breakup of the cavity tip. Visual observations suggested predominantly entrained bubble sizes between 0.5 and 5 mm (see Section 5). Such millimetric size bubbles have a nearly constant bubble rise velocity: i.e.,  $u_r \approx 0.25$ – $0.3$  m/s (Comolet, 1979). At larger speeds, the air cavity developed all around the perimeter and most air was entrained by elongation, stretching and breakup of the ventilated cavity.

### 4.2. Experimental results

In the developing flow region, the distributions of void fraction exhibited smooth, derivative profiles (Fig. 3). Fig. 3 presents typical void fraction data for an impact

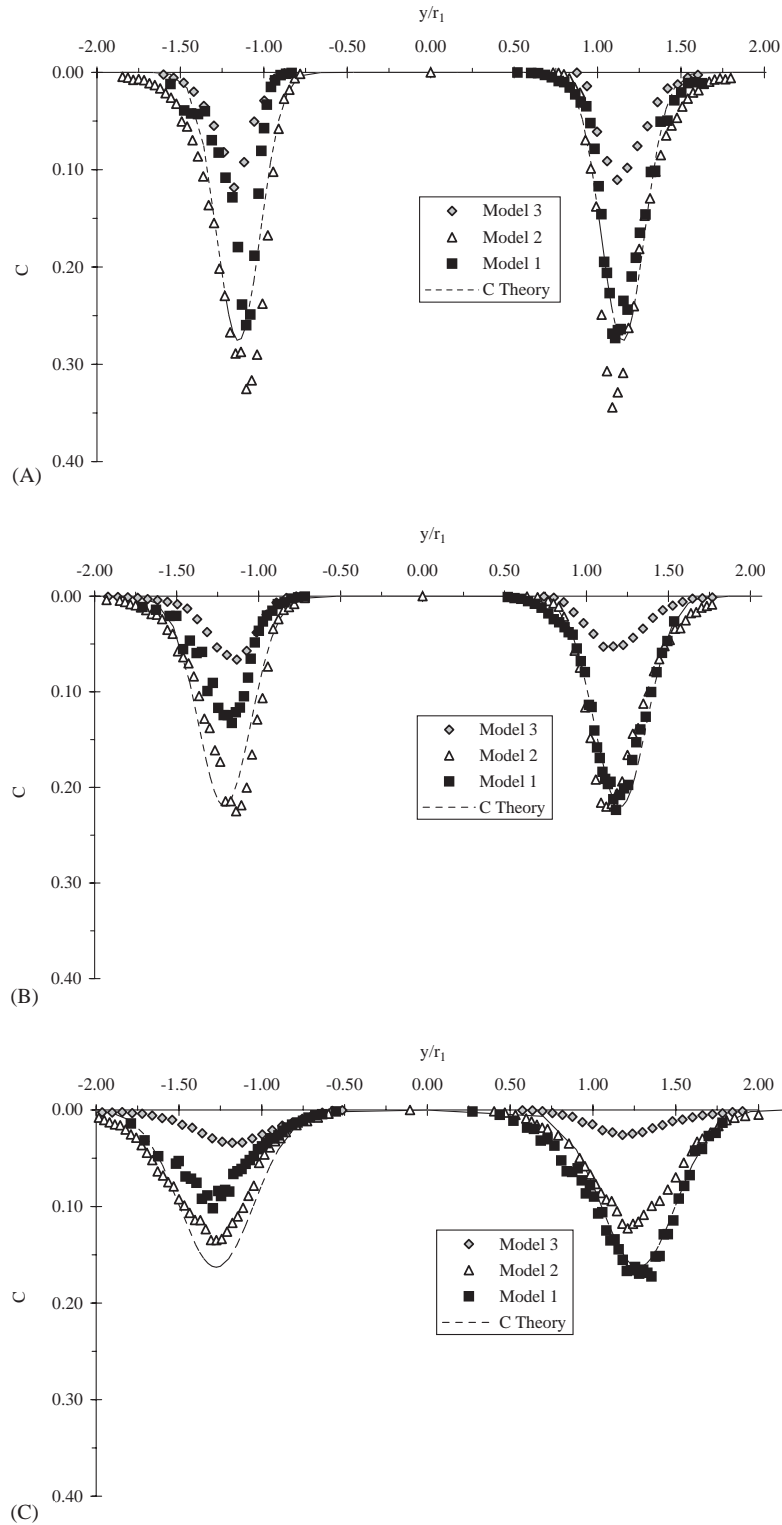


Fig. 3. Distributions of void fraction  $C$  for identical inflow conditions ( $x_1/d_o = 4.0, Fr_1 = 8.5$ )—Comparison between experimental data and Eq. (3) (for Model 1): (A)  $(x - x_1)/d_1 = 1.6$ ; (B)  $(x - x_1)/d_1 = 2.5$ ; (C)  $(x - x_1)/d_1 = 4.1$ .

Froude number  $Fr_1 = 8.5$  and at three cross sections  $(x - x_1)/r_1$ . The data illustrate the advective diffusion of entrained air associated with an quasi-exponential decay of

the maximum air content with longitudinal distance from impingement and a broadening of the air diffusion layer. For all experiments, the data may be fitted by a simple analytical

Table 2  
Characteristics air–water flow measurements in vertical circular plunging jets

$V_1$ (m/s)	$Fr_1$	$\frac{x-x_1}{r_1}$	$\frac{Y_{C_{\max}}}{r_1}$	$C_{\max}$	$\frac{Y_{F_{\max}}}{r_1}$	$\frac{F_{\max}r_1}{V_1}$	$\frac{Q_{\text{air}}}{Q_w}$ <sup>a</sup>	$D^\#$ <sup>a</sup>
(1)	(2)	(3)	(4)	(5)	(6)	(7)	(8)	(9)
<i>Model 1</i>								
3.5	7.2	1.67	1.08	0.23	1.07	0.32	0.108	3.4E–3
		2.51	1.18	0.16	1.12	0.23	0.100	4.0E–3
		4.18	1.18	0.08	1.19	0.16	0.085	6.3E–3
4.1	8.4	1.65	1.11	0.36	1.05	0.38	0.178	5.2E–3
		2.48	1.20	0.23	1.09	0.29	0.174	5.0E–3
		4.13	1.25	0.19	1.14	0.23	0.180	6.0E–3
4.4	9.0	1.64	1.11	0.39	1.06	0.42	0.193	5.0E–3
		2.46	1.17	0.27	1.08	0.34	0.193	5.0E–3
		4.11	1.27	0.19	1.17	0.26	0.180	5.5E–3
<i>Model 2</i>								
2.42	7.1	1.67	1.22	0.21	1.15	0.32	0.160	7.0E–3
		2.51	1.24	0.11	1.19	0.18	0.105	6.5E–3
		4.19	1.38	0.06	1.32	0.11	0.060	6.0E–3
3.04	8.8	1.65	1.09	0.33	1.01	0.40	0.240	6.5E–3
		2.47	1.12	0.22	1.04	0.30	0.200	6.0E–3
		4.11	1.24	0.13	1.14	0.18	0.160	7.2E–3
3.18	9.2	1.64	1.10	0.36	1.02	0.40	0.280	6.5E–3
		2.46	1.14	0.22	1.04	0.32	0.200	7.0E–3
		4.10	1.25	0.15	1.10	0.24	0.190	7.0E–3
3.46	10.0	1.63	1.12	—	1.03	—	0.410	7.0E–3
		2.45	1.05	—	1.05	0.25	0.390	7.0E–3
		4.09	1.29	—	1.10	0.20	0.400	9.0E–3
<i>Model 3</i>								
1.79	7.1	1.69	1.07	0.04	1.04	0.05	0.030	8.0E–3
		2.51	1.10	0.03	1.04	0.05	0.030	8.0E–3
		4.20	1.13	0.02	0.95	0.04	0.031	9.0E–3
2.16	8.5	1.66	1.15	0.11	1.15	0.11	0.070	4.5E–3
		2.48	1.12	0.06	1.09	0.09	0.045	4.0E–3
		4.14	1.18	0.03	1.06	0.05	0.033	5.0E–3
2.30	9.0	1.65	1.17	0.12	1.11	0.14	0.075	4.7E–3
		2.47	1.17	0.08	1.08	0.10	0.060	4.7E–3
		4.12	1.17	0.04	0.99	0.07	0.047	5.5E–3
2.49	9.7	1.65	1.43	0.23	1.32	0.17	0.200	9.0E–3
		2.46	1.39	0.19	1.29	0.15	0.190	8.0E–3
		4.10	1.36	0.10	1.18	0.10	0.155	1.1E–2

Notes: <sup>a</sup> Best fit between Eq. (3) and data; —: not available; *Italic data*: doubtful data.

solution of the advective diffusion equation for air bubbles:

$$C = \frac{Q_{\text{air}}}{Q_w} \frac{1}{4D^\#(x-x_1)/Y_{C_{\max}}} \exp\left(-\frac{1}{4D^\#} \frac{(r/Y_{C_{\max}})^2 + 1}{(x-x_1)/Y_{C_{\max}}}\right) \times I_0\left(\frac{1}{2D^\#} \frac{r/Y_{C_{\max}}}{(x-x_1)/Y_{C_{\max}}}\right), \quad (3)$$

where  $Q_w$  is the water flow rate,  $Q_{\text{air}}$  is the air flux,  $x$  is the longitudinal coordinate,  $D^\#$  is a dimensionless air bubble diffusivity,  $Y_{C_{\max}} = r(C = C_{\max})$  and  $I_0$  is the modified Bessel function of the first kind of order zero (Chanson, 1997). Eq. (3) is compared with Models 1 data in Fig. 3. Values of  $D^\#$  and  $Q_{\text{air}}/Q_w$  were determined from best fit and summarised in Table 2 (Columns 8 and 9).

Distributions of bubble count rates are presented in Fig. 4 for the same inflow conditions and similar cross sections as in Fig. 3. For all experiments, the results highlighted a maximum bubble frequency in the developing shear layers. In Table 2, observed values of maximum void fraction  $C_{\max}$  and maximum bubble count rate  $F_{\max}$  are summarised in columns 5 and 7, respectively, while their respective radial locations  $Y_{C_{\max}}$  and  $Y_{F_{\max}}$  are presented in columns 4 and 6. The maximum bubble count rate occurred consistently in the inner shear region, i.e., at a distance  $Y_{F_{\max}}$  from the jet centreline that was smaller than the location  $Y_{C_{\max}}$  where the void fraction was maximum. Such a result was previously observed with two-dimensional jets (Brattberg and Chanson, 1998), although it is not properly understood.

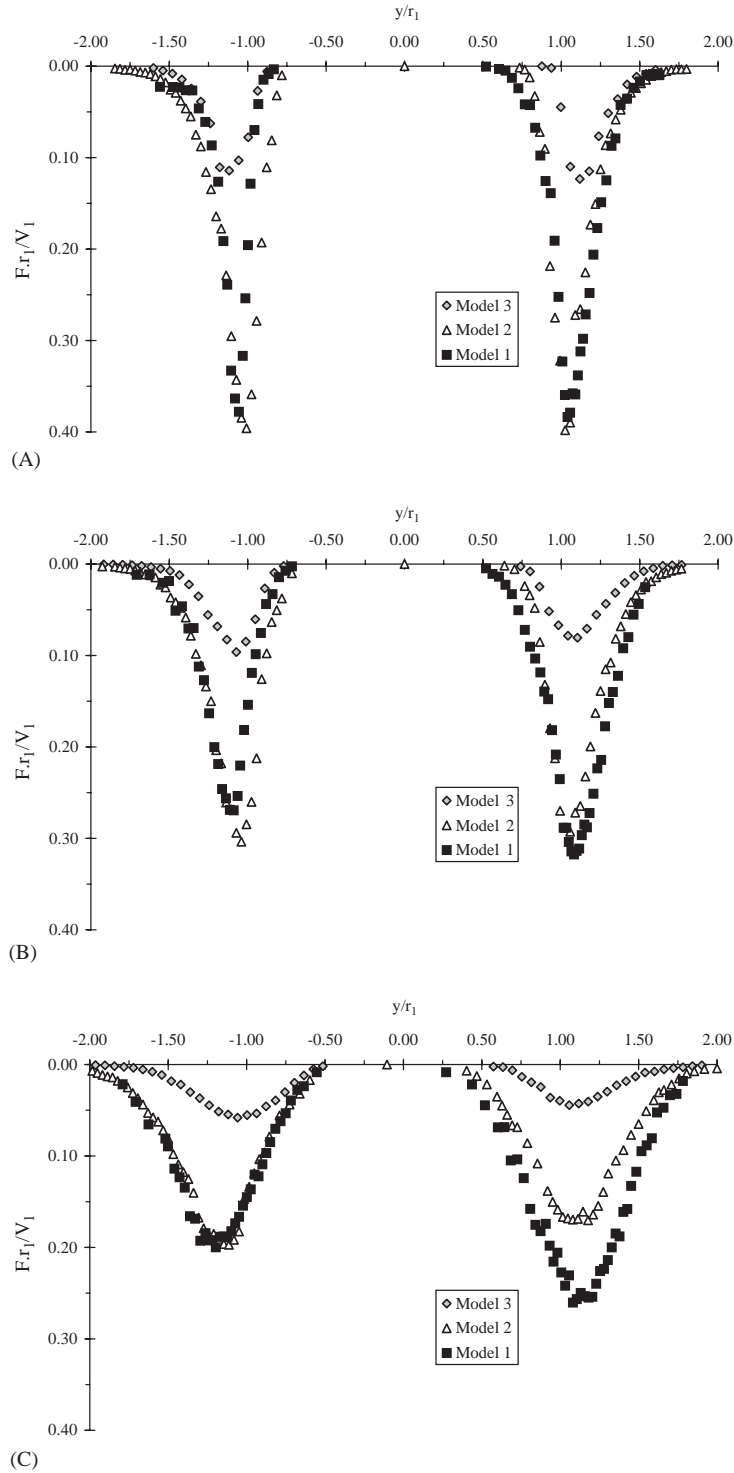


Fig. 4. Distributions of dimensionless bubble count rate  $Fr_1/V_1$  for identical inflow conditions ( $x_1/d_o = 4.0, Fr_1 = 8.5$ ): (A)  $(x - x_1)/d_1 = 1.6$ ; (B)  $(x - x_1)/d_1 = 2.5$ ; (C)  $(x - x_1)/d_1 = 4.1$ .

### 4.3. Discussion. Scale effects

With identical fluids (air and water) in all models, the physical modelling based upon Froude similitude implies that the Weber number differs between experiments and that surface tension-dominated processes might not be properly

scaled. In the present study, Model 3 data showed consistently lesser entrained air than the two larger models (Models 1 and 2). That is, lesser void fractions and lesser dimensionless bubble count rates for identical inflow conditions (Figs. 3 and 4). The observations imply that the rate of air entrainment was underestimated in Model 3. Hence Model 3

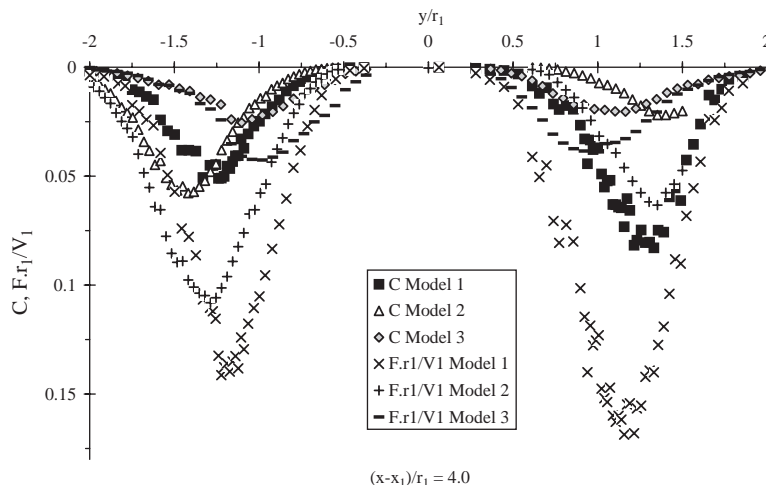


Fig. 5. Dimensionless distributions of void fraction and bubble count rate for identical inflow conditions ( $x_1/d_o = 4.0, Fr_1 = 7$ ) at  $(x - x_1)/r_1 = 4$ .

experiments were affected by scale effects for full-scale, prototype dimensions such that  $d_1 > 10$  mm. For the range of investigated flow conditions (Table 1), the scale effects were observed for  $We_1 < 1E + 3$  where  $We_1$  is the inflow Weber number.

Identical results were basically observed between Models 1 and 2 at each cross section for  $Fr_1 = 8.5$  and 9. Some differences were noted however for the lowest Froude number ( $Fr_1 = 7$ ) (Fig. 5). That is, a faster decay of void fraction and bubble count rate with increasing distance  $(x - x_1)/r_1$  in Model 2. This is illustrated in Fig. 5, showing dimensionless distributions of void fraction and bubble count rate at  $(x - x_1)/r_1 = 4$  for  $Fr_1 = 7$ . Model 2 data exhibit there smaller void fractions and dimensionless count rates than for the larger Model 1. The trend suggests a greater detrainment rate in Model 2, possibly because the observed rise velocity was nearly identical in all models and the bubble rise velocity cannot be scaled with a Froude similitude. Based upon the present study, it is suggested that some scale effect in terms of detrainment occurs for  $V_1/u_r < 10$  and  $We_1 > 1E + 3$ , where  $u_r$  is the characteristic rise velocity of entrained air bubbles.

*Remarks:* For the lowest Froude number ( $Fr_1 = 7$ ), the void fraction and bubble count rate distributions showed some disymmetry which might be attributed to a feedback mechanism between the probe support and developing vortices. For  $r > 0$ , the probe support interfered with both sides of the developing shear region, preventing the development of helicoidal vortical structures. In turn, air entrapment was affected.

## 5. Distributions of bubble chord sizes

### 5.1. Presentation

Bubble chord time data are presented in terms of pseudo-bubble chord length  $ch_{ab}$  (Eq. (1)) in Fig. 6 and

Table 3. In Fig. 6, each figure shows the normalised probability distribution function of pseudo-chord length  $ch_{ab}$  where the histogram columns represent the probability of chord length in 0.5 mm intervals, e.g., the probability of a chord length from 2.0 to 2.5 mm is represented by the column labelled 2.0. The last column (i.e.  $> 10$ ) indicates the probability of chord lengths exceeding 10 mm. Each histogram describes all bubbles detected in a cross section (i.e. 8 locations) at depths  $(x - x_1)/r_1 = 1.65$  and 4.1 for Figs. 6A and B, respectively. The statistical properties of pseudo-chord length distributions are summarised in Table 3: the number of samples is listed in column 4 while the mean and standard data are given in columns 5 and 6, and the skewness and kurtosis are listed in columns 7 and 8, respectively. The results highlight that the mean pseudo-chord sizes were between 4 and 7 mm. That is, there was predominance of millimetric entrained bubbles for all the models.

For all investigated inflow conditions, the data demonstrated the broad spectrum of pseudo-bubble chord lengths at each cross section: i.e., from less than 0.5 mm to larger than 10 mm (Fig. 6). The pseudo-bubble chord length distributions were skewed with a preponderance of small bubble sizes relative to the mean. The probability of bubble chord length was the largest for bubble sizes between 0 and 2 mm although the mean pseudo-chord size was typically 4.1 to 9.1 mm (Table 3, Column 5). The trends were emphasised by positive skewness and large kurtosis (Table 3, Columns 7 and 8). Note the large fraction of bubbles larger than 10 mm next to the impingement perimeter: that is, for  $(x - x_1)/r_1 = 1.62$  (Fig. 6A). These large bubbles may be large air packets entrapped at impingement which were subsequently broken up by turbulent shear. For a given experiment, the data (Fig. 6, Table 3) showed consistently a decrease in mean chord size and standard deviations, as well as skewness and kurtosis, with increasing distance from impingement. For example, compare Figs. 6A and B. The trend was consistent

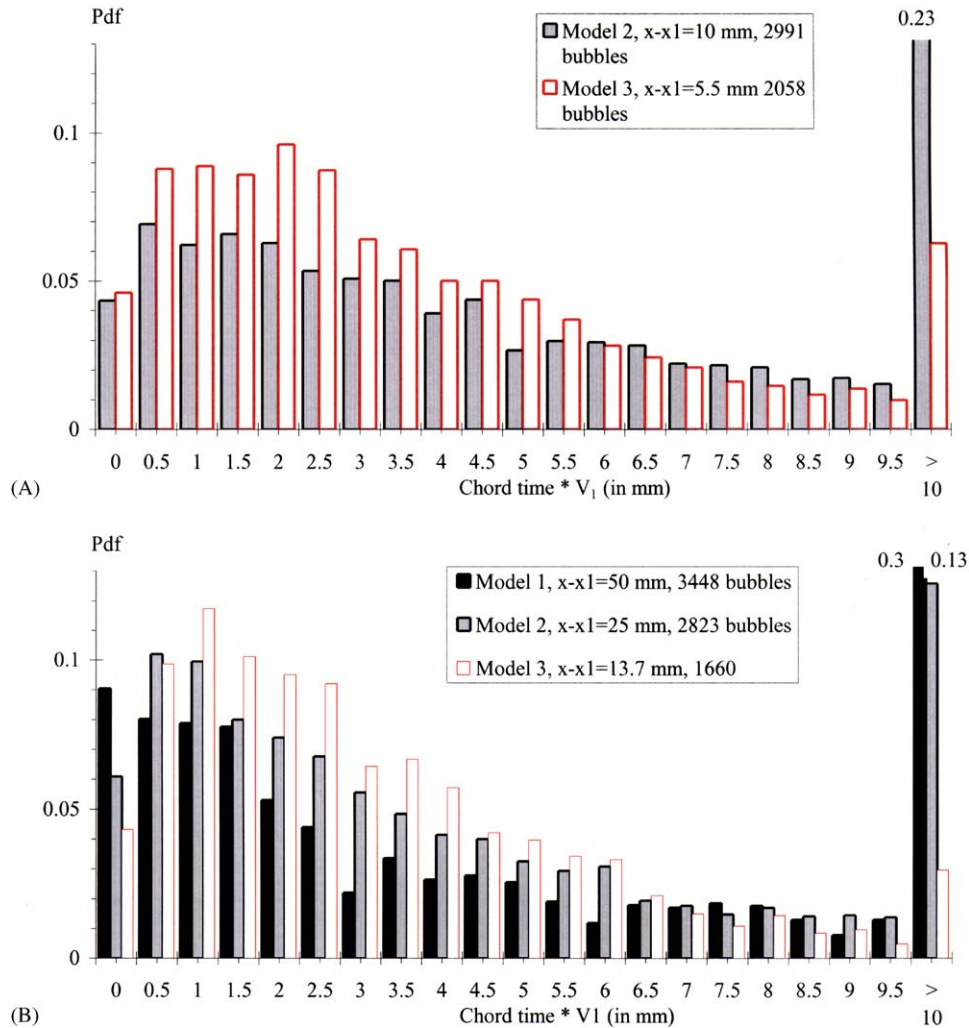


Fig. 6. Pseudo-bubble chord length distributions ( $ch_{ab} = V_1 t_{ch}$ ) –  $Fr_1 = 9, x_1/d_o = 4$ —Comparison between Models 1–3 data: (A)  $(x - x_1)/r_1 = 1.65$ ; (B)  $(x - x_1)/r_1 = 4.1$ .

with the observations of Cummings and Chanson (1997b, 1999) and Brattberg and Chanson (1998) in the developing flow region of two-dimensional plunging jet flows.

The distributions of pseudo chord sizes were compared with “classical” statistical distributions. The data were possibly best fitted by a log-normal distribution confirmed by a  $\chi^2$  goodness-of-test fit, although both Gamma and Weibull distributions provided also good fit. Overall it was not possible to single out any of these three distributions for the investigated flow conditions.

### 5.2. Comparison between geometrically similar models

Figs. 6A and B compare pseudo-bubble chord length distributions for similar inflow conditions between Model 1 ( $d_o = 25$  mm), Model 2 ( $d_o = 12.5$  mm) and Model 3 ( $d_o = 6.8$  mm). The experimental results showed that mean chord sizes were consistently smaller in Model 3 than in the

larger Model 2, while the mean chord size was smaller in Model 2 than in Model 1 for one data set. It is worth noting that the number of entrained bubbles with pseudo-chord size larger than 10 mm was basically negligible in Model 3. The result was consistent with the observations of lesser void fraction in the smallest model for identical inflow conditions (e.g. Fig. 3). Further standard deviation and kurtosis were significantly larger in Model 2 than in Model 3 at a similar cross section.

The comparative results showed drastically a lesser entrainment of both large ( $ch_{ab} > 10$  mm) and small ( $ch_{ab} < 1$  mm) bubbles in the smallest Model 3 (Fig. 6). That is, the pseudo-chord size distribution of entrained bubbles was not scaled according to the geometric scaling ratio between Model 3 and Models 1 nor 2. For one data set ( $Fr_1 = 9, (x - x_1)/r_1 = 4$ ), the data showed further that the mode decreased with increasing jet sizes (Fig. 6B). In Fig. 6B, the mode is within 0–0.5, 0.5–1 and 1–1.5 mm for Models 1, 2 and 3, respectively. Overall, the data

Table 3  
Measured means and standard deviations of pseudo chord length  $ch_{ab}$

$V_1$ (m/s)	$Fr_1$	$\frac{x - x_1}{r_1}$	Nb of bubbles	Mean $ch_{ab}$ (mm)	Std $ch_{ab}$ (mm)	Skewness	Kurtosis	Remarks
(1)	(2)	(3)	(4)	(5)	(6)	(7)	(8)	(9)
<i>Model 1</i>								
4.4	9.0	4.11	3448	9.37	12.12	2.32	7.16	Scan duration: 20 s at 25 kHz. Probe sensor size: 0.35 mm.
<i>Model 2</i>								
2.42	7.1	4.19	1371	4.48	4.31	2.44	9.22	Scan duration: 20.4 s at 25 kHz. Probe sensor size: 0.1 mm.
3.04	8.8	4.11	2517	4.92	5.12	2.55	10.59	
3.18	9.2	1.64	2999	7.40	8.96	3.40	17.08	
		2.46	3341	5.79	6.45	3.10	15.89	
3.46	10.0	4.10	2887	4.93	5.33	2.76	12.93	
		4.09	3421	6.27	7.14	2.68	10.05	
<i>Model 3</i>								
2.32	9.1	1.65	2058	4.07	3.64	2.41	9.56	Scan duration: 20.4 s at 25 kHz. Probe sensor size: 0.1 mm.
		2.47	1940	3.61	3.08	2.19	7.69	
		4.12	1660	3.45	2.80	2.01	7.12	

Notes: Nb of bubbles: number of samples (column 4); Mean  $ch_{ab}$ : mean pseudo-bubble chord length (column 5); Std  $ch_{ab}$ : standard deviation of pseudo-chord length (column 6); Skewness: Fisher skewness of pseudo-chord length (column 7); Kurtosis: Fisher kurtosis of pseudo-chord length (column 8).

highlight that bubble size distributions were not scaled properly based upon a Froude similitude.

## 6. Summary and conclusion

Air entrainment at vertical circular plunging jets was investigated for a range of flow conditions (Table 1). The project was focused on scale effects affecting air entrainment and bubble dispersion. Three scale models were used with jet nozzle diameters of 6.8, 12.5 and 25 mm. Detailed air–water measurement were performed systematically based upon a Froude similitude.

The study of air entrainment inception conditions showed that the inception velocity  $V_e$  was comparable to previous studies. For jet velocities greater than the onset velocity (i.e.  $V_1 > V_e$ ), the distributions of void fraction in the developing flow region followed closely an analytical solution of the advection diffusion equation for air bubbles. The results highlighted significant scale effects in terms of void fraction and bubble count rate when  $We_1 < 1000$ , where  $We_1$  is the inflow Weber number. Model studies with  $We_1 < 1000$  will underestimate air entrainment when prototype flow conditions satisfy  $We_1 > 1000$ . Conversely, large-size laboratory studies ( $d_1 > 10$  mm) will overestimate air entrainment in small size prototypes ( $d_1 < 7$  mm). For  $We_1 > 1000$ , the data suggested also a faster detrainment rate with increasing distance from impingement for  $V_1/u_r < 10$ , where  $V_1$  is the jet impact velocity and  $u_r$  is the bubble rise velocity.

Measured distributions of pseudo-bubble chord sizes showed a broad range of entrained bubbles, with mean pseudo-chord sizes between 4 and 9 mm (Table 3). The distributions were skewed with a preponderance of small

bubbles. The bubble size distribution shape was close to Log-normal, Gamma and Weibull distributions. For one series of experiments ( $Fr_1 = 9$ ), the results suggested a lesser entrainment of both large and small bubbles in the smallest Model ( $d_o = 6.8$  mm).

Overall the study demonstrated scale effects in air entrainment of vertical circular plunging jets. Further studies of the developing flow region should investigate air–water velocity distributions and turbulent velocity fluctuations.

## Notation

$C$	air concentration defined as the volume of air per unit volume of air and water; it is also called void fraction
$C_{\max}$	maximum air concentration in the air bubble diffusion layer
ch	chord length, m
$ch_{ab}$	pseudo-bubble chord length, m, defined as: $ch_{ab} = V_1 t_{ch}$
$d$	jet diameter (m) measured perpendicular to the flow direction
$d_{ab}$	air bubble diameter, m
$d_o$	jet nozzle diameter, m
$d_1$	jet diameter (m) at the impact with the receiving pool of liquid
$D_t$	turbulent diffusivity ( $m^2/s$ ) of air bubbles in air–water flow
$D^\#$	dimensionless turbulent diffusivity: $D^\# = D_t/(V_1 r_1)$
$F$	air bubble count rate (Hz) defined as the number of detected air bubbles divided by the scanning time

$F_{\max}$	maximum bubble frequency (Hz) at a given cross section
$Fr$	Froude number defined as $Fr = V/\sqrt{gd_1}$
$Fr_1$	impingement Froude number $Fr_1 = V_1/\sqrt{gd_1}$
$Mo$	Morton number defined as $Mo = g\mu_w^4/(\rho_w\sigma^3)$
$Q_w$	water discharge, m <sup>3</sup> /s
$Q_{\text{air}}$	air discharge, m <sup>3</sup> /s
$r$	radial distance (m) from the centreline
$r_1$	jet radius (m) at impingement point (e.g. of plunging jet)
$Tu$	turbulence intensity defined as $Tu = u'/V$
$t$	time, s
$t_{\text{ch}}$	bubble chord time (s) defined as the time spent by the bubble on the probe tip
$u_r$	bubble rise velocity, m/s
$u'$	root mean square of longitudinal component of turbulent velocity, m/s
$V$	velocity, m/s
$V_e$	onset velocity (m/s) for air entrainment
$V_1$	impingement velocity, m/s
$We_1$	Weber number at impingement $We_1 = \rho_w V_1^2 d_1 / \sigma$
$x$	distance along the flow direction, m
$x_1$	streamwise distance (m) between the channel intake and the impingement point
$Y_{C_{\max}}$	distance (m) normal to the support where $C = C_{\max}$
$Y_{F_{\max}}$	distance (m) normal to the support where $F_{ab} = (F_{ab})_{\max}$

### Greek letters

$\mu$	dynamic viscosity, Pa s
$\rho$	density, kg/m <sup>3</sup>
$\sigma$	surface tension between air and water, N/m

### Subscripts

air	air flow
w	water flow
1	upstream flow conditions: e.g. impinging jet flow conditions immediately upstream of impact

### Other symbol

$\emptyset$	diameter, m
-------------	-------------

### Acknowledgements

The authors acknowledge the financial support of the Australian Academy of Science, Japan Society for the Promotion of Science and Ministry of Education, Culture, Sports, Science and Technology, Japan. H. Chanson and S. Aoki thank their students for assistance: Mr. B. Bolden, Mr C. Hinton, Mr. Iwata, Ms Kida, Mr T. McGibbon, and Mr C. Proctor. They acknowledge the helpful comments of

Dr T. Suzuki (TUT), Dr Y. Yasuda (Nihon University), and Dr R. Manasseh (CSIRO).

### References

- Bin, A.K., 1993. Gas entrainment by plunging liquid jets. *Chemical Engineering Science* 48 (21), 3585–3630.
- Bonetto, F., Lahey Jr., R.T., 1993. An experimental study on air carryunder due to a plunging liquid jet. *International Journal of Multiphase Flow* 19 (2), 281–294 (Discussion: Vol. 20(3), pp. 667–770).
- Brattberg, T., Chanson, H., 1998. Air entrapment and air bubble dispersion at two-dimensional plunging water jets. *Chemical Engineering Science* 53(24), pp. 4113–4127. Errata: 1999, 54(12), 1925.
- Brennen, C., 1970. Cavity surface wave patterns and general appearance. *Journal of Fluid Mechanics Part I* 44, 33–49.
- Chanson, H., 1988. A study of air entrainment and aeration devices on a spillway model. Ph.D. Thesis, Ref. 88-8, Department of Civil Engineering, University of Canterbury, New Zealand.
- Chanson, H., 1997. Air Bubble Entrainment in Free-surface Turbulent Shear Flows. Academic Press, London, UK, 401pp.
- Chanson, H., 1999. The Hydraulics of Open Channel Flows: An Introduction. Butterworth-Heinemann, Oxford, UK, 512pp.
- Chanson, H., Brattberg, T., 1996. Air–water bubbly flow in free-shear layers. *Proceedings of the 1996 ASME Fluids Engineering Conference, San Diego, USA, ASME-FED Vol. 236, Vol. 1, pp. 357–364.*
- Chanson, H., Brattberg, T., 1998. Air entrainment by two-dimensional plunging jets: the impingement region and the very-near flow field. *Proceedings of the 1998 ASME Fluids Engineering Conference, FEDSM'98, Washington DC, USA, June 21–25, Paper FEDSM98-4806, 8pp. (CD-ROM).*
- Chanson, H., Aoki, S., Hoque, A., 2002. Similitude of air bubble entrainment and dispersion in vertical circular plunging jet flows. An experimental study with freshwater, salty freshwater and seawater. *Coastal/Ocean Engineering Report, No. COE02-1, Department of Architecture and Civil Engineering, Toyohashi University of Technology, Japan, 94pp.*
- Comolet, R., 1979. Sur le Mouvement d'une bulle de gaz dans un liquide (gas bubble motion in a liquid medium). *Journal La Houille Blanche* (1), 31–42 (in French).
- Cummings, P.D., Chanson, H., 1997a. Air entrainment in the developing flow region of plunging jets. Part 1 theoretical development. *Journal of Fluids Engineering, Transactions of the ASME* 119 (3), 597–602.
- Cummings, P.D., Chanson, H., 1997b. Air entrainment in the developing flow region of plunging jets. Part 2 experimental. *Journal of Fluids Engineering, Transactions of the ASME* 119 (3), 603–608.
- Cummings, P.D., Chanson, H., 1999. An experimental study of individual air bubble entrainment at a planar plunging jet. *Chemical Engineering Research and Design, Transaction of IChemE, Part A* 77 (A2), 159–164.
- Ervine, D.A., McKeogh, E.J., Elsayy, E.M., 1980. Effect of turbulence intensity on the rate of air entrainment by plunging water jets. *Proceedings, Institution of Civil Engineers (Part 2) Vol: 69, pp. 425–445.*
- Goldring, B.T., Mawer, W.T., Thomas, N., 1980. Level surges in the circulating water downshaft of large generating stations. *Proceedings of the Third International Conference on Pressure Surges, BHRA Fluid Engineering, F2, Canterbury, UK, pp. 279–300.*
- Henderson, F.M., 1966. *Open Channel Flow*. MacMillan Company, New York, USA.
- Hoyt, J.W., Taylor, J.J., 1977. Waves on water jets. *Journal of Fluid Mechanics Part I* 83, 119–127.
- Hughes, S.A., 1993. Physical models and laboratory techniques in coastal engineering. In: *Advanced Series on Ocean Engineering, Vol. 7. World Scientific, Singapore.*

- Iino, M., Suzuki, M., Ikushima, A.J., Okuda, Y., 1985. Surface tension of liquid  $^3\text{He}$  down to 0.3 K. *Journal of Low Temperature Physics* 59 (3/4), 291–294.
- Kennedy, B.S., Burley, R., 1977. Dynamic fluid interface displacement and prediction of air entrainment. *Journal of Colloid and Interface Science* 62 (1), 48–62.
- Knapp, R.T., Daily, J.W., Hammitt, F.G., 1970. *Cavitation*. McGraw-Hill Book Company, New York, USA.
- Kobus, H. (Ed.), 1984. *Proceedings of International Symposium on Scale Effects in Modelling Hydraulic Structures*, IAHR, Esslingen, Germany.
- McKeogh, E.J., 1978. A study of air entrainment using plunging water jets. Ph.D. Thesis, Queen's University of Belfast, UK, 374pp.
- McKeogh, E.J., Irvine, D.A., 1981. Air entrainment rate and diffusion pattern of plunging liquid jets. *Chemical Engineering Science* 36, 1161–1172.
- Robison, R., 1994. Chicago's waterfalls. *Civil Engineering*, ASCE 64 (7), 36–39.
- Sene, K.J., 1984. Aspects of bubbly two-phase flow. Ph.D. Thesis, Trinity College, Cambridge, UK, December.
- Sene, K.J., 1988. Air entrainment by plunging jets. *Chemical Engineering Science* 43 (10), 2615–2623.
- Van de Donk, J., 1981. Water aeration with plunging jets. Ph.D. Thesis, TH Delft, The Netherlands, 168pp.
- Wood, I.R., 1991. Air entrainment in free-surface flows. *IAHR Hydraulic Structures Design Manual No. 4. Hydraulic Design Considerations*, Balkema, Rotterdam, The Netherlands, 149pp.
- Yasuda, Y., 2001. Personal communication, November 1.
- Zhu, Y.G., Oguz, H.N., Properetti, A., 2000. On the mechanism of air entrainment by liquid jets at a free surface. *Journal of Fluid Mechanics* 404, 151–177.